Journal of Minerals and Materials Characterization and Engineering, 2023, 11, 172-196
https://www.scirp.org/journal/jmmce
ISSN Online: 2327-4085
ISSN Print: 2327-4077

Influence of the Partial Substitution of Industrial Clinker by Volcanic Lava Powder from Nyiragongo Volcano on the Physical Properties of Mortars

Seke Vangu Max[1,2*], Clement Nzau Umba Di Mbudi[3], Makanzu Imwangana Fils[3,4,5], Seke Makunga Daudet[6], Efoto Eale Louis[1]

[1]Department of Physics and Technology, Faculty of Science and Technology, University of Kinshasa, Kinshasa, The Democratic Republic of the Congo
[2]Faculties of Engineering & Architecture, Kongo University, Mbanza-Ngungu, The Democratic Republic of the Congo
[3]Department of Geosciences, Faculty of Sciences and Technologies, University of Kinshasa, Kinshasa, The Democratic Republic of the Congo
[4]Centre of Research on Geology and Mining, Laboratory of Geomorphology and Remote Sensing, Kinshasa, The Democratic Republic of the Congo
[5]National Institute of Building and Public Works, INBTP, Kinshasa, The Democratic Republic of the Congo
[6]Sibanye-StillWater Ltd., Johannesburg, South Africa
Email: *max.seke.@unikin.ac.cd, *maxseke@gmail.com

How to cite this paper: Max, S.V., Mbudi, C.N.U.D., Fils, M.I., Daudet, S.M. and Louis, E.E. (2023) Influence of the Partial Substitution of Industrial Clinker by Volcanic Lava Powder from Nyiragongo Volcano on the Physical Properties of Mortars. *Journal of Minerals and Materials Characterization and Engineering*, **11**, 172-196.
https://doi.org/10.4236/jmmce.2023.115014

Received: July 31, 2023
Accepted: September 11, 2023
Published: September 14, 2023

Abstract

This study evaluates the pozzolanicity of Nyiragongo volcano lava flows in Congo by an indirect method using mortars with different rock powder proportions. The clinker used is a locally produced alite clinker, whose chemical and mineralogical composition was determined by XRF, Bogue and Taylor formulas. The lava flows were collected from the 2002, 2010 and 2021 eruption sites, and were characterized by XRF, CIPW normative mineralogy and geomechanical tests. The results show that Nyiragongo rocks are ultrabasic, silica- and alkali-rich, and contain minerals like nepheline, wollastonite and leucite. They satisfy the natural pozzolan criterion, and have pozzolanic activity indices above 70%. These rocks also have high RC and LA resistances, ranging from 190 MPa to 45 MPa, and from 18% to 32.6%, respectively. The rock powder addition in the mortars reduces mechanical resistances and increases setting times, except for a 5% replacement rate, which speeds up hardening. Nyiragongo lava can be used as a pozzolanic addition to produce a CEM II/B-P 32.5 cement.

Keywords

Pozzolan, Cement, Alite, Nyiragongo, ASR (Alkali-Silica Reaction)

1. Introduction

Portland clinker production is an energy-intensive industrial process that emits a lot of greenhouse gases. The increasing demand for cement leads to an increase in air pollution, as the cement industry is responsible for about 8% of anthropogenic CO_2 emissions [1]. To reduce the environmental impact of cement production, it is necessary to use reactive mineral additions, of natural or artificial origin, that can partially replace Portland clinker. This substitution allows to decrease the clinker/cement ratio and thus the CO_2 emissions, without compromising the performance of the cement product [2] [3]. Reactive mineral additions have hydraulic and/or pozzolanic properties [4] [5]. They have been studied by researchers since the 1970s [6] [7]. They present advantages such as: the reduction of the heat of hydration, the improvement of the durability of the cementitious material, the prevention and repair of alkali-aggregate reactions, the improvement of the workability and long-term mechanical strength, the improvement of the resistance to sulfate attacks [8]-[13].

An energetic advantage of natural pozzolans over artificial pozzolans is that they do not require prior thermal treatment to activate their reactivity. In DRC, in the east of the country, the Virunga chain contains eight volcanoes, two of which are active (Nyiragongo and Nyamulagira) and six inactive (Gahina, Mikeno, Visoke, Karisimbi, Muhavura and Sabinyo) [14] [15]. The Nyiragongo rock as a pozzolan, substitute for clinker, in cement industry is poorly documented in the literature. Geochemical studies of the magmatism of Nyiragongo volcano [16]-[23] indicate that these rocks are basalts close to trachy-basalts. Other works [24] [25] [26] [27] show that basalts in partial replacement of clinker improve the mechanical and physico-chemical properties of the cementitious material. Basalt increases in particular the physico-chemical properties of cementitious mortar and a good fineness of grinding favors the mechanical properties by accelerating the hydration kinetics [28] [29] [30] [31]. The basaltic rock having a proven pozzolanic property and the geochemistry of Nyiragongo basalt being sufficiently studied in the literature, we conducted this study to determine the effectiveness of Nyiragongo basaltic rock as a "supplementary cementitious material". We chemically characterized three different lava flows (2002, 2010 and 2021) by XRF radio-analyses, we evaluated the influence of partial substitution of clinker by Nyiragongo basalt at progressive rates of 5%, 10%, 15%, 20% and 25% on setting times, and we followed the variation of mechanical strengths related to them, comparing them to the control mortar. We thus determined the pozzolanicity of Nyiragongo rock, its application for cement purposes and the class of resulting cement at 25% substitution according to CEM II/B-P.

2. Materials & Methods

The materials used in this study are as follows: the industrial clinker, which is the main component of cement; the gypsum, which acts as a setting regulator; the Nyiragongo volcanic rock, which is used as a pozzolanic material in partial replacement of clinker; and the local standardized sand, which forms the granular skeleton of the mortar. The clinker and gypsum were supplied by HeidelbergCement Group Cilu-RDC plant, while the Nyiragongo volcanic rock was sampled in the Goma region, located in the east of the Democratic Republic of Congo (DRC), where the active volcano of the same name is located (Figure 1). The local standardized sand was collected in Muanda, on the west coast of the country.

2.1. Materials

2.1.1. Clinker

The clinker used of alite nature is produced on the industrial site of the LUKALA cement plant (HeidelberCement Group Cilu-RDC plant). These nodules are micronized in a laboratory ball mill by co-grinding with gypsum and mineral addition.

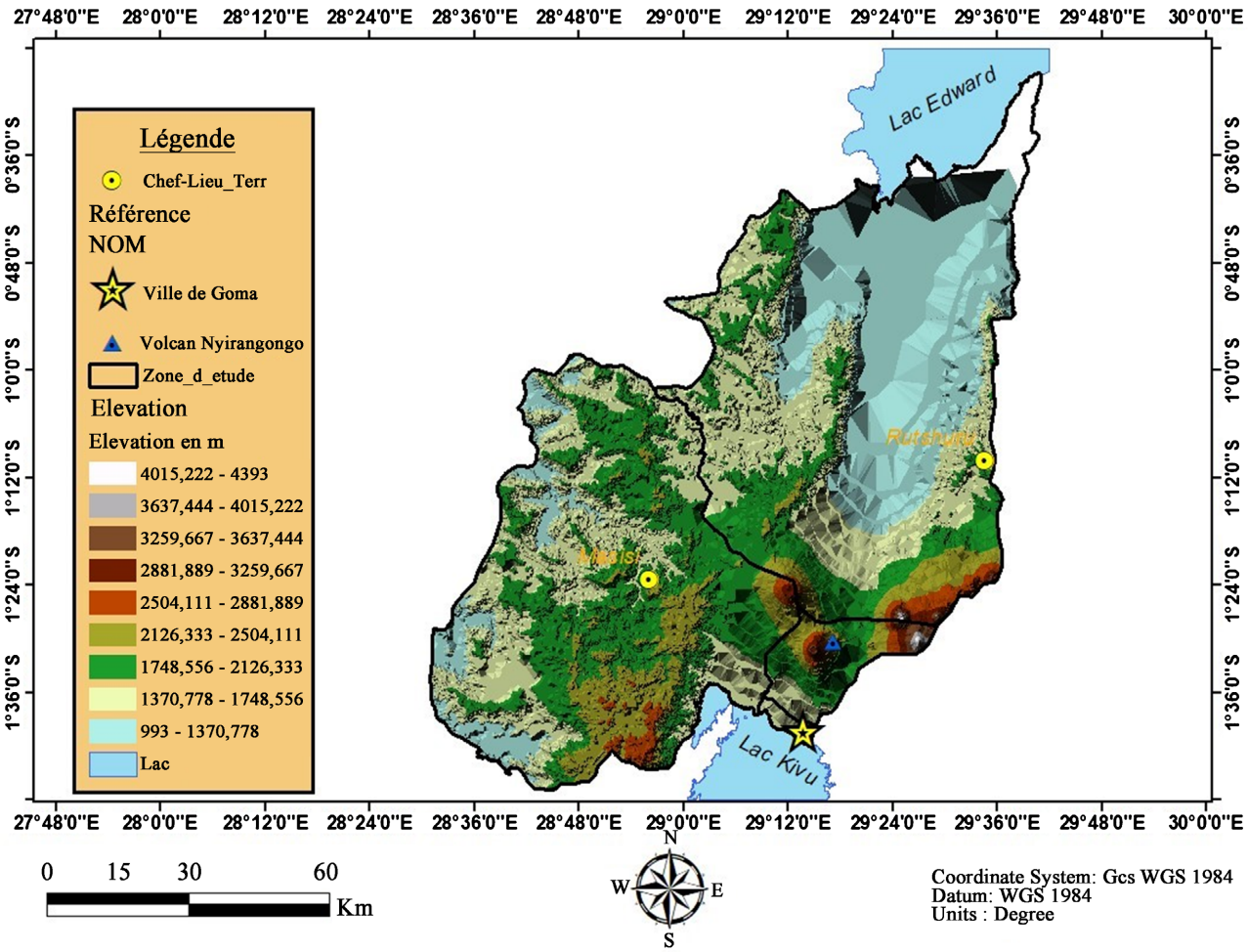

Figure 1. Mapping of the Nyiragongo study area.

2.1.2. Cement

The cement used is a variant of ordinary Portland cement taken as a reference, the composite cement is obtained by substitutions of Clinker at progressive rates and co-ground with gypsum.

2.1.3. Nyiragongo Rock

The sampling of this rock covers the different flows of 2002, 2010, 2021. According to the mapping of **Figure 1**; this rock, which is the subject of a pozzolanic study.

2.1.4. Mixing Water

The mixing water used in the HeidelberCement Group Cilu-RDC laboratory is distilled water.

2.1.5. Local Standardized Sand

The fine sand of LUILA and the moderately coarse sand of NSIAMFUMU constituted the mixture of a siliceous sand conforming to the standard sand standard.

2.2. Methods

The ASTM C 618 [32] assesses the volcanic rock powder based on the chemical and physical requirements of pozzolanicity, while the NF EN ISO 17892-7 [33] measures the compressive strength of rocks. The mortars are made with different amounts of powder, following the water and aggregate ratios defined by the NF EN 1008 standard [34] [35]. The mortars are tested for their properties when fresh and hardened according to the following standards: NF EN 196-1 [36], NF EN 196-3 [37] [38], NF EN 192-6 [39] and NF EN 1097-2 [40] [41].

2.2.1. Formulation and Tests

Table 1 of mortar formulations presents the proportions of clinker, basalt, gypsum, sand and water to be used to produce mortars with different rates of substitution of clinker by basalt powder. The table shows that the total amount of clinker and basalt remains constant (436.5 g), as well as that of gypsum (13.5 g), sand (1350 g) and water (225 ml). The table will lead to evaluate the effect of the substitution of clinker by basalt on the physical properties of mortars, such as setting time, compressive strength and consistency. The table suggests that the

Table 1. Cement formulation for fresh mortar 4 * 4 *16 cm^3.

Formulation	Clinker (gr)	Basalt (gr)	Clinker & Basalt (gr)	Gypsum (gr)	Sand (gr)	Water (ml)
M-0%	450	0	436.5	13.5	1350	225
M-5%	427.5	22.5	436.5	13.5	1350	225
M-10%	405	45	436.5	13.5	1350	225
M-15%	382.5	67.5	436.5	13.5	1350	225
M-20%	360	90	436.5	13.5	1350	225
M-25%	337.5	112.5	436.5	13.5	1350	225

use of basalt as a natural pozzolan could reduce the consumption of clinker and thus the environmental impact of cement production.

2.2.2. Cement Paste Setting Test

The Setting Test of the cement paste is followed in accordance with the requirements of the standard on a multi-position automatic prisometer [37].

To evaluate the setting times (start and end) of the control and reformulated mortars with basalt at progressive substitution rates, the standard used leads to a formulation for the paste to be tested that are shown in Table 2.

2.2.3. Geomechanical and Radio-Analyses Tests

1) Los Angeles

The aggregates were crushed in the 10 - 25 granular class according to the relevant standard whose elements are presented in Table 3.

The Los Angeles test is a method to measure the weight percentages of elements having a size smaller than 1.6 mm, which are produced by the fragmentation of 5 kg of the tested material after being subjected to the impacts of standardized balls in a cylinder for 500 rotations during 15 minutes. The classes are defined for the Los Angeles test (for specific applications) as follows: Class A: LA < 30; Class B: 30 < LA < 35; Class C: 35 < LA < 40; Class D: 40 < LA < 50.

2) Uniaxial compressive strength [39]

The compressive strength test, also called RC, is the uniaxial compressive stress measured at the complete failure of the studied material; this stress is divided by the area of the offered surface. The classification of the rock is made possible by Table 4.

3) Microscopy and Spectroscopy (Fluorescence/FTIR)

a) Optical Microscopy

Optical mineralogy allowed us to analyze the Nyiragongo rocks and their minerals according to their optical properties in thin section. The observation presented in (Figure 2) was performed with an optical microscope in polarized light analyzed (PLA) and in polarized light not analyzed (PLNA). Optical

Table 2. Cement paste formulation for setting time.

Composition	M_0 100% - 0%	M_5 95% - 5%	M_{10} 90% - 10%	M_{15} 85% - 15%	M_{20} 80% - 20%
Water (ml)	132 gr	132 gr	132 gr	132 gr	132 gr
Cement	500 gr	500 gr	500 gr	500 gr	500 gr
Water/Cement	0.264	0.264	0.264	0.264	0.264

Table 3. Los angeles test [40].

Granular class (mm)	Fraction granular	Number of cannonballs	Total weight of the load	Weight of the fractions (g)
10 - 25	10 - 16	11	4840 ± 25	3000
	16 - 25			2000

Table 4. Uniaxial compressive strength of rocks.

Description	RC (MPa)	Example
Very low	1 to 25	chalk, salt
Low	25 to 50	coal, limestone, schist
Average	50 to 100	sandstone, slate, claystone
High	100 to 200	marble, granite, gneiss
Very high	>200	quartzite, Basalt

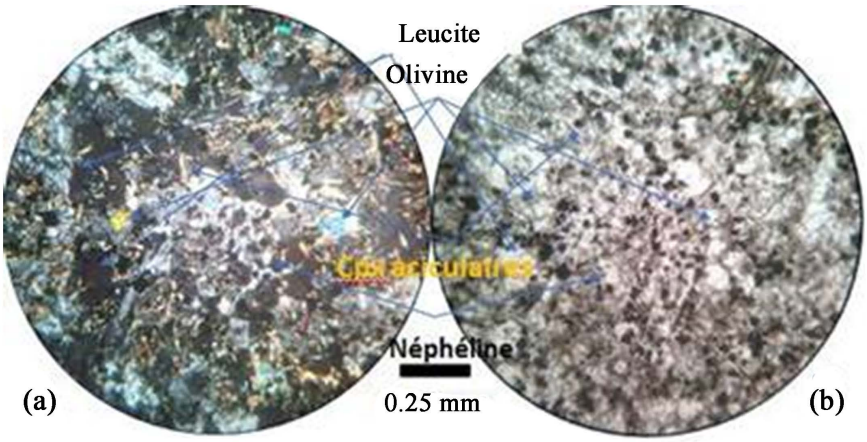

Figure 2. Thin Sections of Nyiragongo lava with minerals.

microscopy has limitations in terms of resolution, subjectivity and time required to identify volcanic rocks, which are more heterogeneous and complex than plutonic rocks [42]. This work shows that optical microscopy is simple and fast, but limited by the resolution and preparation of the samples, to work sharply powder X-ray diffraction is precise and quantitative, but requires optimal experimental conditions and complex data analysis. However, powder X-ray diffraction is more suitable for the identification of crystalline phases, which may require other techniques as volcanic rocks cool quickly.

b) The FTIR

The analysis by Fourier transform infrared spectroscopy of the local standardized sand allows to verify the absence and to guarantee the non-contribution of amorphous silicas in the granular structure of cementitious matrices (mortars) in accordance with quality requirements. The importance of complementary techniques (XRF, XRD and FTIR) is necessary to analyze the crystalline and amorphous phases of silica in sand.

The Fourier transform Infrared Alpha Bruker spectrophotometer was used to identify the functional groups of the samples. The samples were ground and placed between 400 and 4000 cm^{-1} wavelength range for measurement at Council for Scientific and industrial Research(CSIR) in South Africa/Pretoria. The transmission spectrum showed the crystalline phases and their corresponding functional groups.

c) X-ray Fluorescence Spectroscopy

The elemental composition of the samples was determined by X-ray fluorescence spectroscopy using two instruments: a wavelength dispersive spectrometer (WD-XRF) belonging to the cement manufacturer Heidelberg Cement Group Cilu-RDC and an energy dispersive spectrometer (ED-XRF) located at the CGEA/CRENK laboratory.

At the CGEA/CRENK laboratory, we used ED-XRF spectrometry (XEPOS III, **Figure 3(a)**) with FP-Pellets CGEA and TQ-Pellets Fast methods to measure elements (ions) in pellets. We calibrated the spectrometer with standards ISE870, ISE 890, ISE919, ISE961 and SOIL-7. The spectrometer had four secondary targets: Mo, Al_2O_3, Co and HOPG Crystal of Bragg. The principle was based on X-ray fluorescence of the sample under X-ray beam. We identified and quantified elements by their characteristic peaks in the energy spectrum. We used the Kα1 peak (3.313 Kev) of K and normalized intensities with respect to the scattering peak for calculation. The results are in the table with t-Student confidence interval at $\alpha = 0.95$.

Two methods of sample preparation were used according to the nature of the rocks: fused beads, which reduce matrix and inter-element effects, were used for silicate rocks, while pressed pellets, which are more suitable for carbonate rocks with high loss on ignition, were chosen for the latter [43]-[48]. At the HeidelbergCement Group laboratory/DRC, we used WD-XRF spectrometry (**Figure 3(b)**). The preparation of the samples in fused beads (Glass beads) consisted of mixing 1 g of sample and 9 g of eutectic flux with composition: 66%-$Li_2B_4O_7$/32%-$LiBO_2$/0.5%-LiBr [49] [50] [51], then melting them in a crucible made of Au-Pt alloy (5% - 95%). This method was applied to the samples of Nyiragongo rock, gypsum, clinker and sand. The clinker used was of alite type, characterized by a Lime Saturation Factor (LSF) [52]-[57].

$$\mathrm{LSF}(\text{alitique}) = \frac{\%\mathrm{CaO}}{2.8\%\mathrm{SiO_2} + 1.2\%\mathrm{Al_2O_3} + 0.65\%\mathrm{Fe_2O_3}} > 0.85$$

The LSF is a parameter that allows to control the ratio of the main silicates of

(a) (b)

Figure 3. (a) ED-XRF Spectrometer /XEPOS III [58], (b) WD-XRF Spectrometer/ Bruker S8 Tiger [59] [60].

the clinker and to evaluate the amount of lime available to react with silica, iron-II and alumina, forming thus the bicalcic and tricalcic silicates, as well as the aluminates. A LSF higher than 85% favors the formation of clinkers rich in alite [61]. The mineralogical composition of the clinker can be estimated from the oxide results obtained by XRF, using empirical formulas based on the Bogue Model [62]. However, this estimation presents uncertainties related to the presence of impurities in the mineral phases and to the variability of the cooling of the clinker, which affects the kinetics of mineral formation [52] [63] [64].

According empirical formulas based on the Bogue Model [62], we can write:

$$\begin{bmatrix} C_3S \\ C_2S \\ C_3A \\ C_4AF \end{bmatrix} = \begin{bmatrix} 4.071 & -7.600 & -6.718 & -1.430 \\ -3.072 & 8.600 & 5.068 & 1.079 \\ 0 & 0 & 2.650 & -1.692 \\ 0 & 0 & 0 & 3.043 \end{bmatrix} \begin{bmatrix} CaO \\ SiO_2 \\ Al_2O_3 \\ Fe_2O_3 \end{bmatrix}$$

According to the New Taylor model [65], we can write:

$$\begin{bmatrix} C_3S \\ C_2S \\ C_3A \\ C_4AF \\ CaSO_4 \\ K_2SO_4 \\ Na_2SO_4 \end{bmatrix} = \begin{bmatrix} 4.634 & -8.897 & -7.301 & -1.362 & -3.245 & 2.758 & 4.192 \\ -3.718 & 10.342 & 5.509 & 0.911 & 2.604 & -2.213 & -3.364 \\ 0.118 & -0.371 & 3.665 & -3.950 & -0.082 & 0.070 & 0.106 \\ -0.023 & -0.056 & -0.886 & 5.621 & 0.016 & -0.014 & -0.021 \\ -0.030 & 0.095 & 0.161 & -0.091 & 1.721 & -1.463 & -2.223 \\ 0.052 & -0.151 & -0.122 & 0.018 & -0.036 & 1.881 & 0.047 \\ -0.005 & 0.005 & -0.078 & 0.078 & 0.003 & -0.003 & 2.287 \end{bmatrix} \begin{bmatrix} CaO \\ SiO_2 \\ Al_2O_3 \\ Fe_2O_3 \\ SO_3 \\ K_2O \\ Na_2O \end{bmatrix}$$

Based on the New Taylor model without alkali sulfates [65], we can write:

$$\begin{bmatrix} C_3S \\ C_2S \\ C_3A \\ C_4AF \\ C\overline{S} \end{bmatrix} = \begin{bmatrix} 4.745 & -9.113 & -7.469 & -2.237 & -3.324 \\ -3.844 & 10.579 & 5.750 & 1.734 & 2.692 \\ 0.071 & -0.308 & 3.668 & -4..063 & -0.049 \\ 0.028 & -0.159 & -0.949 & 5.566 & -0.020 \\ 0 & 0 & 0 & 0 & 1.700 \end{bmatrix} \begin{bmatrix} CaO \\ SiO_2 \\ Al_2O_3 \\ Fe_2O_3 \\ SO_3 \end{bmatrix}$$

The classification of magmatic (volcanic) rock samples is based on the oxide contents obtained by XRF, which are reported in the TAS diagram [66]-[71], which allows to distinguish the different types of rocks according to their chemical composition.

d) The approximate Mineralogy by CIPW

The Nyiragongo rock samples 2002, 2010 and 2021 were analyzed by powder fluorescence, moreover, the CIPW (Cross, Iddings, Pirsson, Washington) normative abundances method [72] [73] [74] [75] was applied to the magmatic (volcanic) rock samples to estimate their virtual mineral composition or normative mineralogy.

3. Results and Discussions

3.1. Results on X-Ray Fluorescence

3.1.1. Clinker

From the oxide contents obtained by XRF and presented in **Table 5**, it is possi-

ble to calculate the LSF (Lime saturation Factor) and to estimate the proportions of the mineral phases of the clinker using the empirical formulas of BOGUE and TAYLOR.

LSF = 89%, confirms an alite clinker. Figure 4 shows the comparison of the proportions of the mineral phases of the clinker estimated by the empirical formulas of BOGUE and TAYLOR. It confirms that the clinker is rich in alite, as suggested by the LSF.

The empirical formulas of Bogue and Taylor give:

$$\text{BOGUE:} \begin{bmatrix} C_3S \\ C_2S \\ C_3A \\ C_4AF \end{bmatrix}_{CILU} = \begin{bmatrix} 45.989 \\ 28.5464 \\ 9.2351 \\ 12.4154 \end{bmatrix}$$

The empirical formulas of TAYLOR also point to a clinker with a predominant Alite with alkaline sulfates around 0.4%c.

$$\text{TAYLOR:} \begin{bmatrix} C_3S \\ C_2S \\ C_3A \\ C_4AF \\ C\bar{S} \end{bmatrix}_{CILU} = \begin{bmatrix} 47.4844 \\ 29.9575 \\ 3.49954 \\ 15.20867 \\ 1.377 \end{bmatrix}$$

Table 5. XRF analysis of CILU clinker.

Oxides	SiO_2	Al_2O_3	Fe_2O_3	CaO	MgO	Na_2O	K_2O	SO_3	MnO	P_2O_5	TiO_2
Clinker	22.08	6.09	4.08	64.49	2.11	0.35	0.56	0.81	0.03	0.09	0

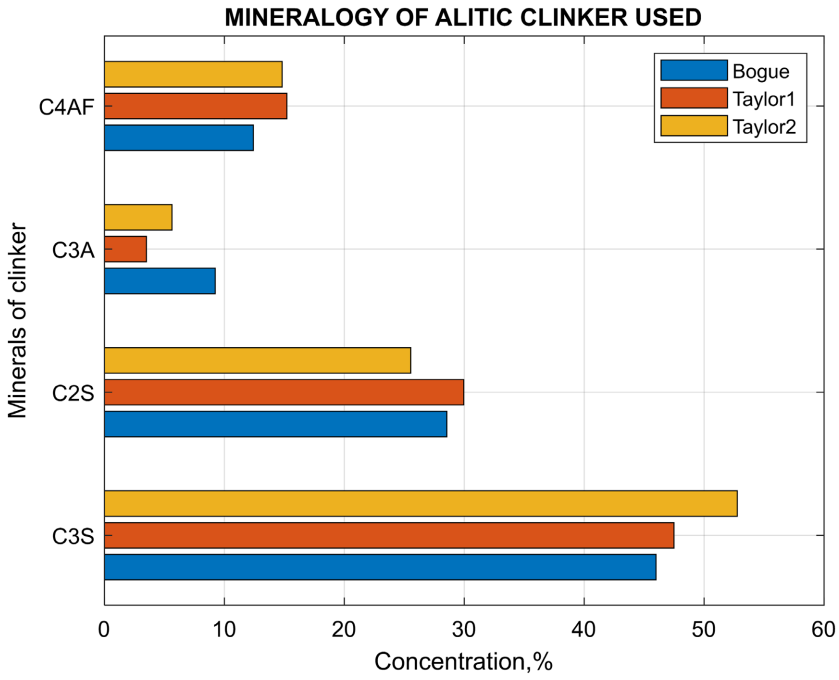

Figure 4. Mineralogy of clinker by Bogue and Taylor.

$$\text{TAYLOR:} \begin{bmatrix} C_3S \\ C_2S \\ C_3A \\ C_4AF \\ CaSO_4 \\ K_2SO_4 \\ Na_2SO_4 \end{bmatrix}_{CILU} = \begin{bmatrix} 52.76408 \\ 25.53679 \\ 5.63187 \\ 14.81596 \\ 0.56879 \\ 0.39051 \\ 0.43237 \end{bmatrix}$$

3.1.2. Nyiragongo Rock

The chemical composition of the Nyiragongo-2002, Nyiragongo-2010 and Nyiragongo-2021 rock, obtained by XRF, allows to classify it in the Total Alkali Silica diagram and to estimate its normative mineralogy with the CIPW software. The oxide contents are represented in the histograms of (**Figure 5**) and (**Figure 6**).

Figure 7 shows the trace element contents of the Nyiragongo-2002 basalt, obtained by XRF-Crenk, and compares them with those of the Noki granite, the Matadi metabasalt and the Mpozo syenite. The Nyiragongo-2002 basalt contains Cu, Zn, Pb, Mo, Sn, Ni, Sr, Nb, Ga and Rb. These elements could indicate the presence of andremeyerite $BaFe^{2+}$ (Si_2O_7), with substitution of Ba by Sr or Zn. This mineral is often encountered in the basalts of Nyiragongo and Nyamulagira [76]. **Figure 8** shows an example of a TAS diagram with the coordinates of the intersection points of the different classification zones.

To evaluate the mineralogical composition of the Nyiragongo rocks, we used a software that applies the CIPW (Cross, Iddings, Pirsson, Washington) model.

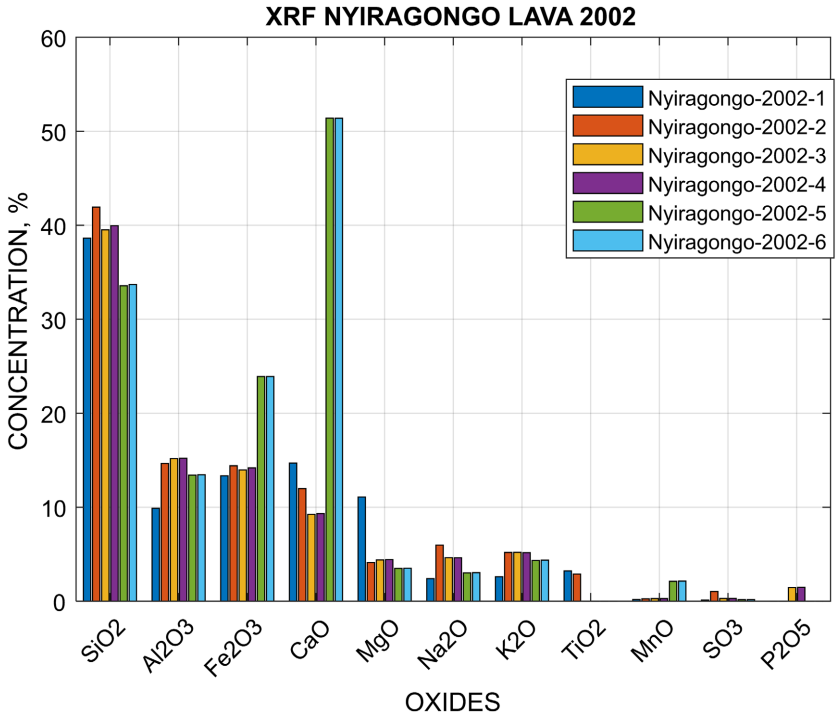

Figure 5. Chemical composition of Nyiragongo lava flow-2002 samples.

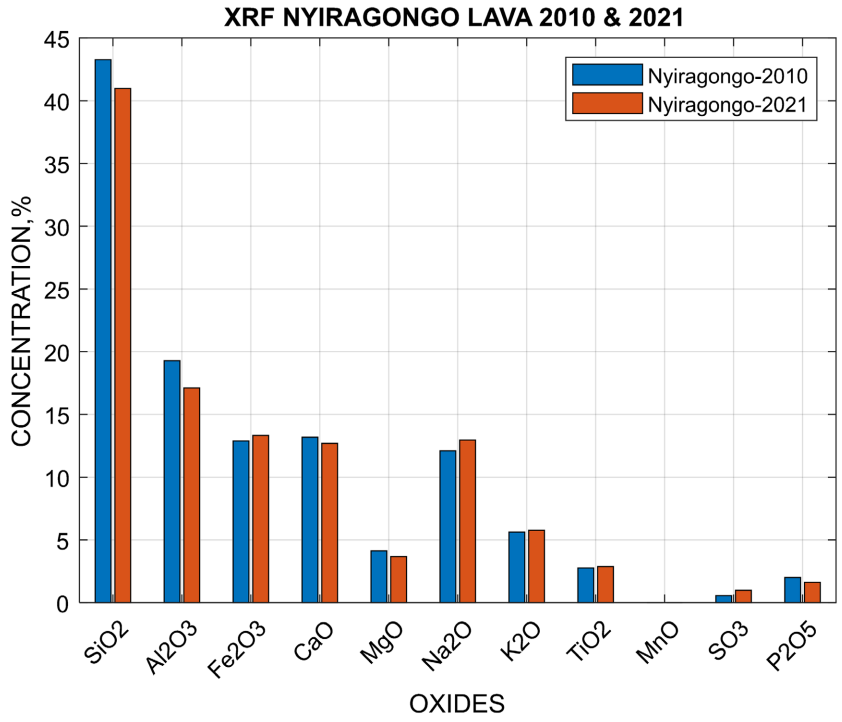

Figure 6. XRF of Nyiragongo lava flows 2010/2021 samples.

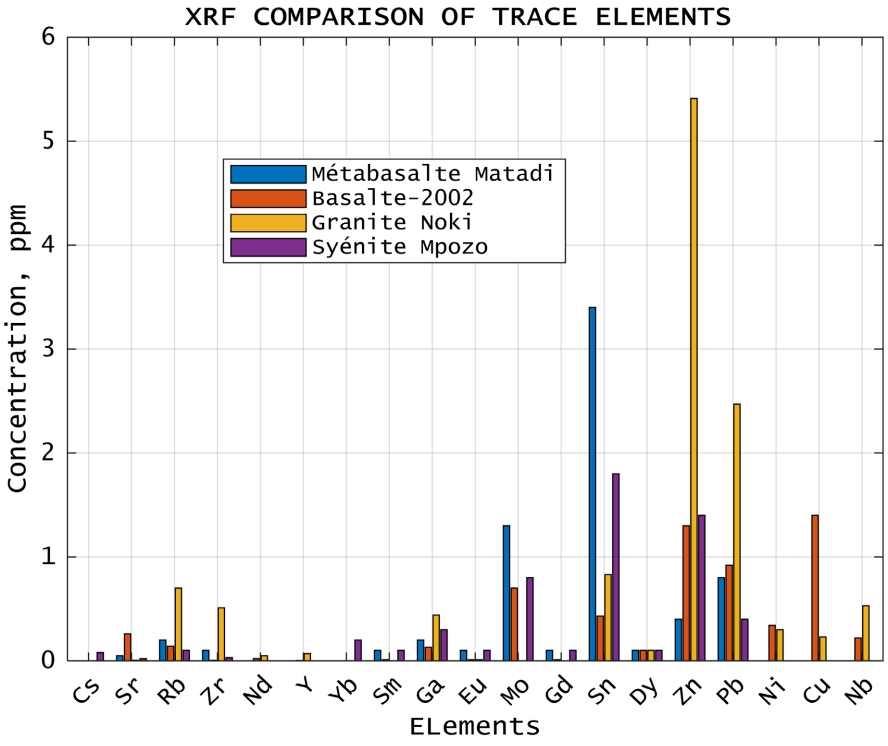

Figure 7. XRF Diagram.

This model allows to determine the proportions of hypothetical minerals that could form a rock from its chemical composition. The software uses XRF (X-ray fluorescence) analyses to measure the oxide content of major and trace elements

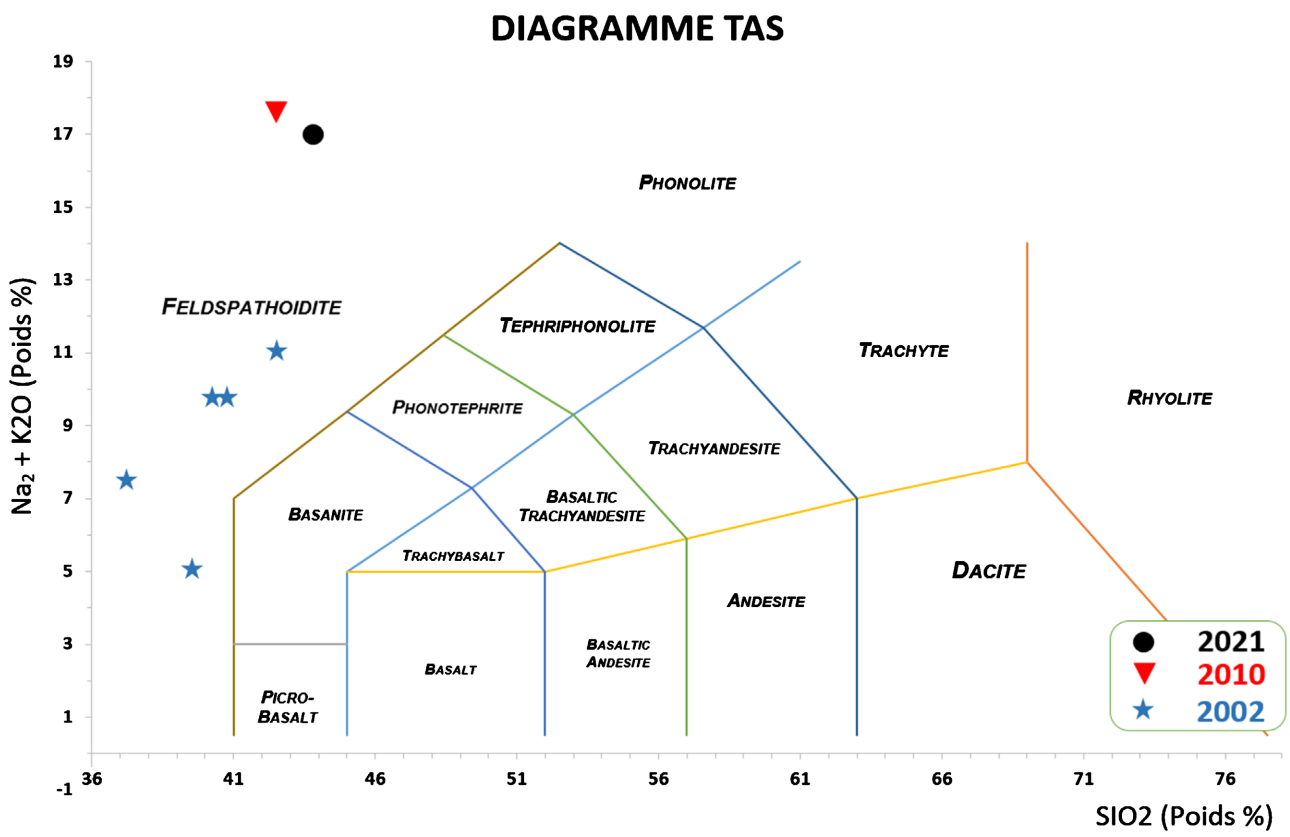

Figure 8. TAS diagram.

Table 6. Mineralogy by CIPW of Nyiragongo rocks.

Mineral	Formula	2002	2010	2021
Aegirine	$NaFe^{3+}Si_2O_6$	3.4%	17.9%	22.9%
Orthoclase	$KAlSi_3O_8$	1.1%	-	-
Leucite	$K_2Al_2Si_4O_{12}$	22.4%	15.4%	15.9%
Nepheline	$Na_2Al_2Si_2O_8$	24.3%	21.7%	17.9%
Olivine	$(Mg,Fe)_2SiO_2$	6.9%	4.2%	-
Perovskite	$CaTiO_3$	4.2%	2.7%	2.9%
Wollastonite	$CaSiO_3$	24.0%	12.9%	13.0%
Hematite	Fe_2O_3	12.7%	1.3%	9.7%
Ilmenite	$FeTiO_3$	0.5%	-	11.5%
Larnite	Ca_2SiO_4	-	9.5%	9.70%
Kaliophilite	$K_2Al_2Si_2O_8$	-	11.1%	-
Apatite	$Ca_{10}P_6F_2O_{24}$	-	2.7%	2.2%
Hypersthene	$FeSiO_3$	-	-	3.8%

in the rocks. Then, it solves a system of algebraic equations to calculate the percentages of normative minerals, such as quartz, feldspar, olivine, etc. Table 6 presents the results obtained by this method for the samples 2002, 2010 and 2021

of the Nyiragongo rocks.

According to Table 6 of CIPW, the rocks 2002, 2010 and 2021 contain minerals that could have an interest as a substitute for clinker, such as: Leucite ($K_2Al_2Si_4O_{12}$) and nepheline ($Na_2Al_2Si_2O_8$), which are aluminous silicates that can react with lime (CaO) to form hydrates of type C-S-H (calcium silicate hydrate) or C-A-S-H (calcium aluminate silicate hydrate), which are the main compounds responsible for the strength of cement. Wollastonite ($CaSiO_3$), which is a calcium silicate that can react with water to form C-S-H, or with tricalcium aluminate (C_3A) to form ettringite ($C_6AS_3H_{32}$), which is a compound contributing to the expansion of cement. Hematite (Fe_2O_3) and ilmenite ($FeTiO_3$), which are iron oxides that can react with lime (CaO) and alumina (Al_2O_3) to form C_4AF, which is a clinker phase having a dark color and a low reactivity. However, these rocks also contain minerals that could have a negative effect as a substitute for clinker, such as: Aegirine ($NaFe^{3+}Si_2O_6$) and olivine ($(Mg,Fe)_2SiO_4$), which are ferromagnesian silicates that can be unstable in air and water, and release ferrous (Fe^{2+}) or magnesian (Mg^{2+}) ions that may cause undesirable secondary reactions, such as the formation of brucite ($Mg(OH)_2$) or magnetite (Fe_3O_4). Perovskite ($CaTiO_3$), which is a titanium oxide that can be inert or react with water to form rutile (TiO_2), which is a very hard and abrasive mineral.

3.1.3. Standardized Sand

Two local sands were chosen and mixed to obtain a local standard sand, conforming to [36]. The XRF analyses show that the silica content of this sand is close to 98%, as required by the standard. Table 7 presents the chemical composition of these two sands in mass percentage of oxides.

In addition to the chemical composition, the particle size distribution of the sand must comply with the standard [36]. Figure 9 shows the particle size distribution curve of the local standard sand, which is in accordance with the standard.

Figure 10 shows the Fourier transform infrared (FTIR) spectrum of this sand, in the mid-infrared (MIR) range from 400 to 4000 cm^{-1}: it mainly shows the characteristic vibration bands of quartz (SiO_2), which are the symmetric stretching band Si-O-Si at 1080 cm^{-1} and the asymmetric stretching band Si-O-Si at 800 cm^{-1} [77].

The sand of Nsiamfumu/Muanda was selected for its particle size distribution similar to that of the standard normalized sands defined by the standard [36], and for its high content of crystalline silica. The presence of some impurities is also noted, such as the C-H stretching band at 2900 cm^{-1}, due to traces of organic

Table 7. Composite & standardized sand used in the analyses at Cilu.

oxides	SiO_2	Al_2O_3	Fe_2O_3	CaO	Na_2O	K_2O	TiO_2	MnO	P_2O_5	MgO	SO_3
Lui.	98.33	0.00	1.23	0.00	0.00	0.28	0.08	0.01	0.00	0.00	0.04
Nsi.	97.65	0.31	1.55	0.00	0.00	0.28	0.06	0.00	0.00	0.06	0.04

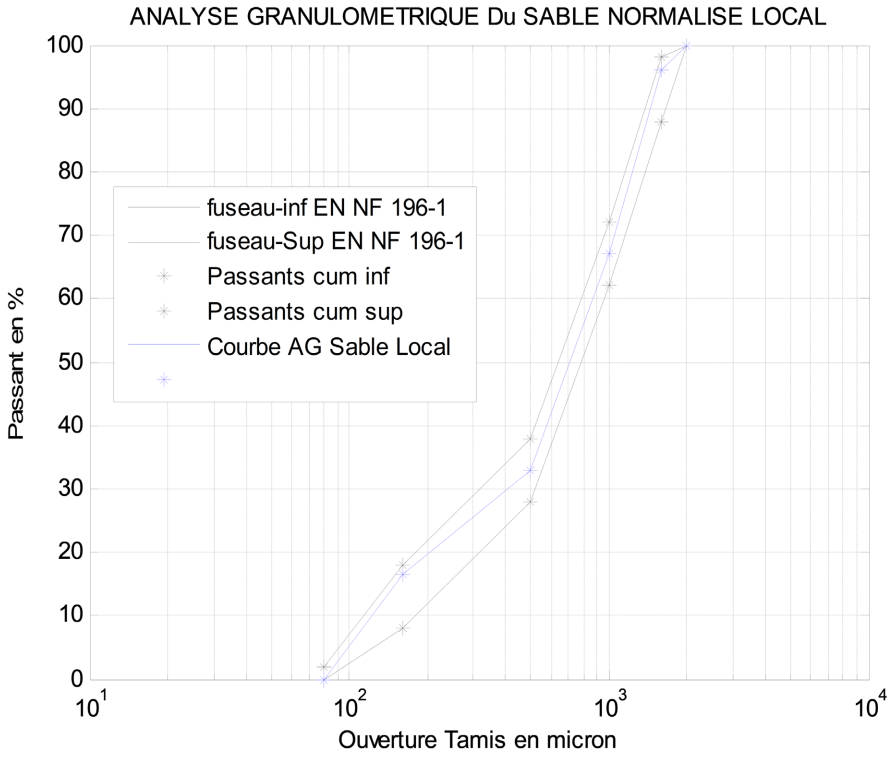

Figure 9. Granulometric analysis of the local standardized sand.

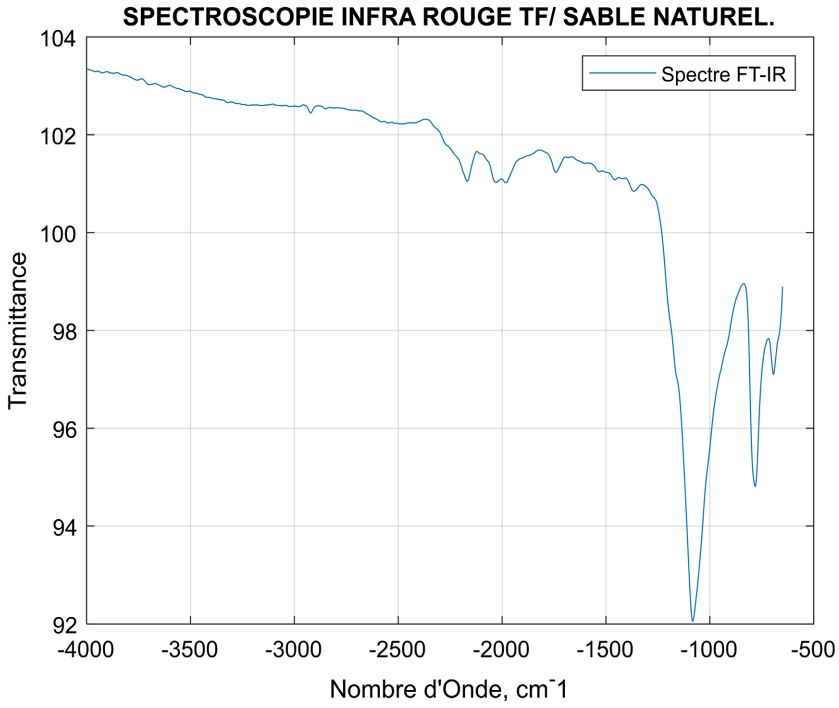

Figure 10. FTIR analysis of the local standardized sand.

matter [78]. The functional group Si-O-Si is the main constituent of quartz, a very hard and abrasion-resistant mineral, which gives the sand its mechanical properties [78] [79]. This group is formed by the covalent bond between two

silicon atoms and one oxygen atom, which forms an angle of 144˚ [80]. The length of the Si-O bond is 1.61 Å, and its strength is 452 kJ/mol [81] [82] [83].

The group Si-O-Si can vibrate symmetrically or asymmetrically, depending on whether the two Si-O bonds lengthen or shorten in phase or out of phase. It can also vibrate in bending, that is, the Si-O-Si angle varies around its equilibrium value. These vibrations are detectable by infrared spectroscopy, because they induce a change in the dipole moment of the group [77]. The functional group O-H is present in water molecules, which can be adsorbed on the surface of the sand by electrostatic interactions or hydrogen bonds. This group is formed by the covalent bond between an oxygen atom and a hydrogen atom, which forms an angle of 104.5˚. The length of the O-H bond is 0.96 Å, and its strength is 467 kJ/mol [81]. The group O-H can vibrate in stretching, that is, the O-H distance varies around its equilibrium value. This vibration is detectable by infrared spectroscopy, because it induces a change in the dipole moment of the group [77]. The functional group C-H is present in organic molecules, which can be contaminants of the sand from natural or anthropogenic sources. This group is formed by the covalent bond between a carbon atom and a hydrogen atom, which forms an angle of 109.5˚ in alkanes, 120˚ in alkenes and 180˚ in alkynes. The length of the C-H bond varies from 1.09 Å to 1.06 Å, and its strength varies from 413 kJ/mol to 839 kJ/mol, depending on the type of hybridization of carbon [84]. The group C-H can vibrate in stretching, that is, the C-H distance varies around its equilibrium value. This vibration is detectable by infrared spectroscopy, because it induces a change in the dipole moment of the group [77]. **Table 8** shows that the M-O-M group has a peak at 1097 cm^{-1}, the M-O group has a peak at 778 cm^{-1} and the MO group has two peaks at 683 cm^{-1} and 414 cm^{-1}. The peak at 683 cm^{-1} corresponds to the symmetric vibration of the MO group, while the peak at 414 cm^{-1} corresponds to the antisymmetric vibration of the same group.

The FTIR spectrum of the sand shows several peaks that correspond to the vibrations of the functional groups present in the material. These vibrations are due to the changes in the dipole moment of the chemical bonds when they are subjected to infrared radiation [85]. The peak at 1097 cm^{-1} is attributed to the symmetric stretching vibration of the Si-O-Si bonds of quartz, which is the main constituent of sand. This vibration occurs when the two oxygen atoms bonded to the same silicon atom move away from or towards the silicon simultaneously [65]. The peak at 778 cm^{-1} is attributed to the asymmetric stretching vibration of the Si-O-Si bonds of quartz. This vibration occurs when the two oxygen atoms bonded to the same silicon atom move in opposite directions with respect to the

Table 8. Peaks.

Peaks (cm^{-1})	1097	778	683
Functional Group	M-O-M MO	M-O Symmetric	MO

silicon [77]. The peak at 683 cm^{-1} is attributed to the bending vibration of the Si-O-Si bonds of quartz. This vibration occurs when the Si-O-Si angle varies around its equilibrium value of 144˚ [80].

3.2. Rock Geomechanics (Los Angeles and Uniaxial Compression Strength), Setting Time, Compressive Strength and Pozzolanicity

Table 9 and Figure 11 show the results of the uniaxial compressive strength and abrasion (Los Angeles) tests performed on basalt samples of grain size class 10 - 25 for three different eruptions: 2002, 2010 and 2021.

Table 9 shows that the basalt has lost abrasion resistance after the eruptions, as indicated by the increase of its Los Angeles (LA) coefficient from 18% in 2002 to 32.60% in 2021. The basalt has therefore become more brittle and produces more fines under shock. Its class has changed from A to B between 2010 and 2021, which affects its quality and suitability for certain applications. For example, road construction requires aggregates of class A or B, with a LA coefficient lower than 30% [86]. The production of rock wool uses basalts of class C, with a LA higher than 30%, but the cement industry prefers a rock that is easy to grind and reactive.

Table 9. Los Angeles Test on Crushed Basalt-Goma.

Description	2002	2010	2021
Los Angeles coefficient	18%	25%	32.60%
Material class	CLASS A	CLASS A	CLASS B

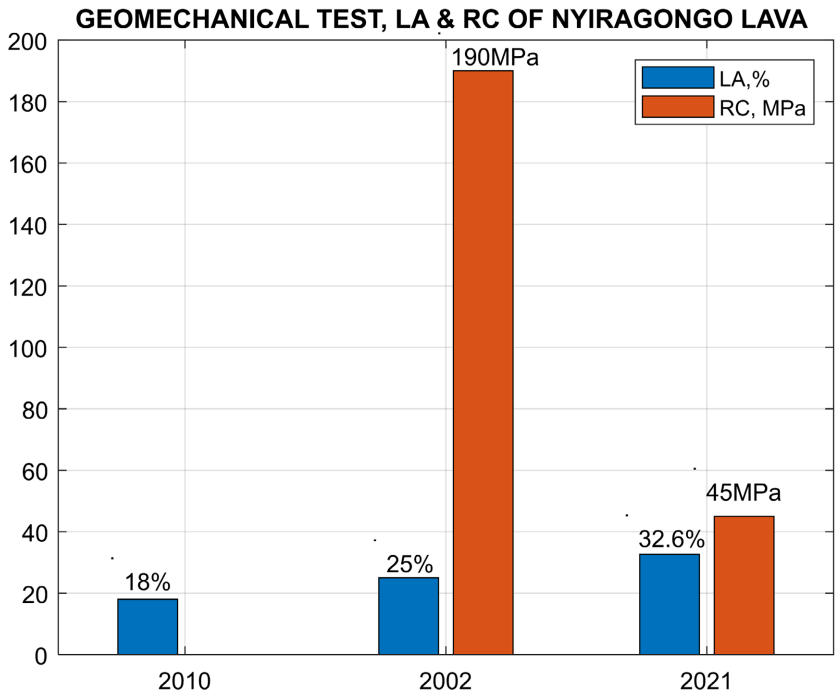

Figure 11. Los Angeles Test on Nyiragongo rocks.

Figure 12 shows the setting times of the mortars with the 2002 rock according to the cement substitution rates. Only the 5% rate does not cause any setting delay. Figure 13 shows the compressive strengths of the standard mortars with the

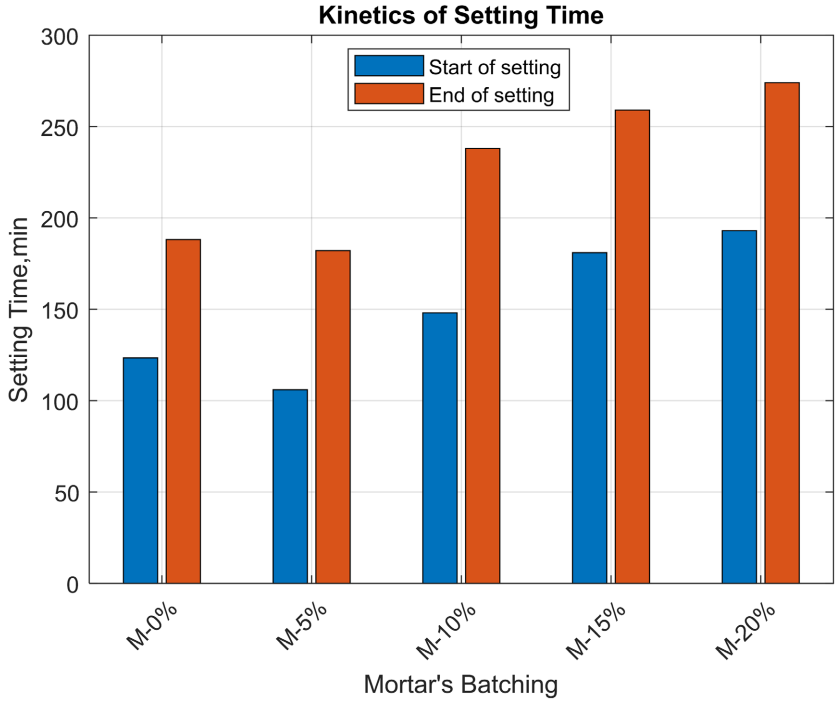

Figure 12. Comparison of the setting time of the mortar with the percentage of replacement of the pozzolan.

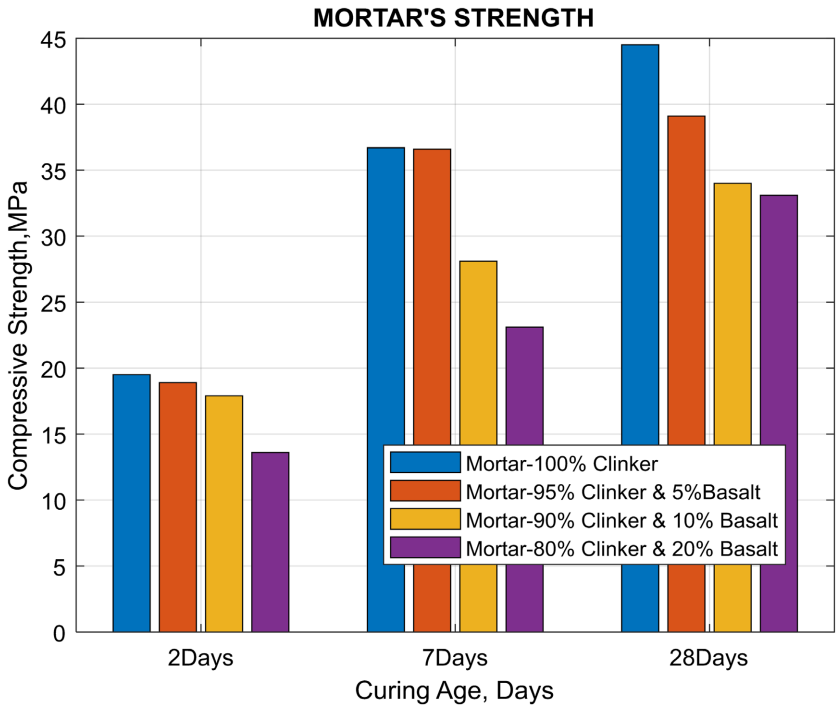

Figure 13. Comparison of the compressive strength of the mortar with the percentage of replacement of the pozzolan as a function of the curing age.

2002 rock at 2, 7 and 28 days. Figure 14 illustrates the effect of the cement replacement rate by a pozzolan and the curing age on the strengths of the mortars on 2, 7, 14 and 28 days. The pozzolanic activity of Nyiragongo was evaluated by indirect method, in witch 25% of Clinker was replaced. The indirect method is used, which consists of measuring the compressive strength of mortar specimens containing the pozzolanic material after 28 days of curing.

3.3. Pozzolanic Activity

The pozzolanic activity index (PAI) is a parameter that evaluates the ability of a material to react with the lime released by the hydration of cement and to form resistant hydrated compounds. According to the ASTM C-618 standard [32], the PAI is calculated as the ratio between the compressive strength at 28 days of a mortar containing 25% of the material in substitution of cement and that of a reference mortar without substitution. Table 10 shows the evolution of the PAI of basalt-Goma, a volcanic rock from the region of the Nyiragongo volcano in DRC, as a function of the curing age of the mortars. It is observed that the PAI of basalt-Goma increases with the curing time, and reaches 76.7% at 28 days, which exceeds the minimum value of 67% required by this standard to qualify a

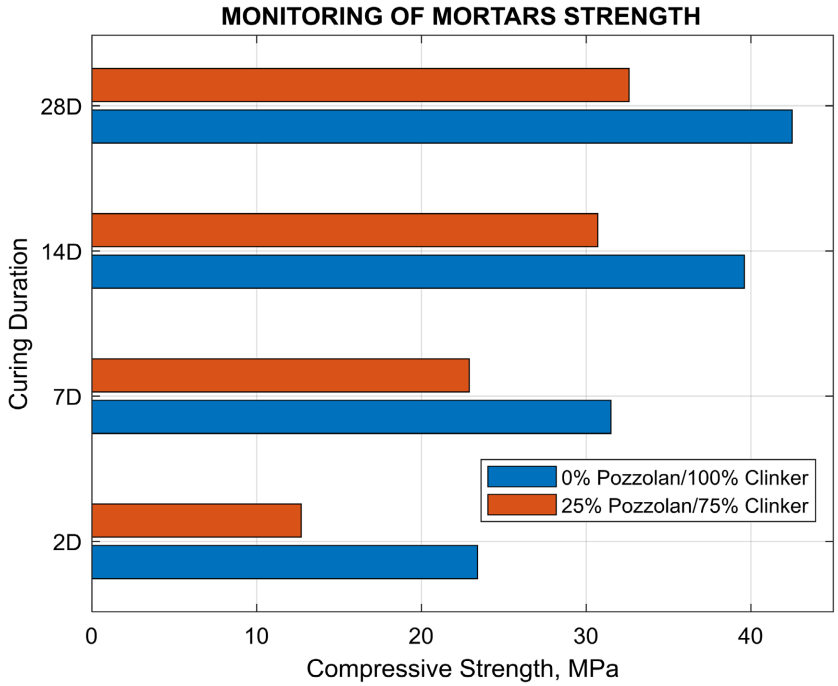

Figure 14. Comparison of the compressive strength of the mortars as a function of the percentage of substitution of the cement by a pozzolanic material and the curing time.

Table 10. Pozzolanicity index of mortars based on basalt 100 - 0 and 75 - 25.

Pozzolanic activity index Basalt-Goma				
Curing time (Days)	**2D**	**7D**	**14D**	**28D**
(Rp/R0) * 100	54.3%	72.7%	77.5%	76.7%

material as pozzolanic. This result indicates that basalt-Goma has sufficient pozzolanic activity to be used as a mineral addition in concrete and mortars.

4. Conclusion

This study revealed the potential of Nyiragongo rock as a natural pozzolan for the development of a low environmental footprint and high performance cement. Nyiragongo rock showed high pozzolanic reactivity, ability to fix alkali sulfates and to compensate for the lack of clays in cement. A Portland composite cement with pozzolan specified CEM II/B-P 32.5N. The use of this cement will lead to the realization of robust, workable and durable cementitious materials, adapted to the context of aggressive environments. The local natural siliceous sand reformulated was also found to be suitable for the composition of mortars. This cement offers a specific interest for hydraulic infrastructure projects in DRC, as it reduces the environmental impact of cement production and it can prevent and treat the pathology RAG (Alkali-Aggregate Reaction) that compromises the reliability of hydroelectric concrete structures. This study opens up research perspectives on the optimization of the formulation of cement based on Nyiragongo rock and on its long-term behavior under mechanical and chemical stresses.

Conflicts of Interest

The authors declare no conflicts of interest regarding the publication of this paper.

References

[1] Andrew, R.M. (2019) Global CO_2 Emissions from Cement Production, 1928-2018. *Earth System Science Data*, **11**, 1675-1710. https://doi.org/10.5194/essd-11-1675-2019

[2] Aïtcin, P.C. (2000) Cements of Yesterday and Today: Concrete of Tomorrow. *Cement and Concrete Research*, **30**, 1349-1359. https://doi.org/10.1016/S0008-8846(00)00365-3

[3] Qizi, A.H.S. and Barotaliyevna, C.N. (2023) Cements of Yesterday and Today: Concrete of Tomorrow. *American Journal of Engineering, Mechanics and Architecture*, **1**, 18-21. https://grnjournal.us/index.php/AJEMA/article/view/279

[4] Mehta, P.K. (1987) Natural Pozzolans: Supplementary Cementing Materials in Concrete. *CANMET Special Publication*, **86**, 1-33.

[5] Nicoara, A.I., Stoica, A.E., Vrabec, M., Šmuc Rogan, N., Sturm, S., Ow-Yang, C., Gulgun, M.A., Bundur, Z.B., Ciuca, I. and Vasile, B.S. (1954) End-of-Life Materials Used as Supplementary Cementitious Materials in the Concrete Industry. *Materials*, **13**, Article 1954. https://doi.org/10.3390/ma13081954

[6] Neville, A.M. (1995) Properties of concrete. Longman, London.

[7] Mohammed, G.A. and Al-Mashhadi, S.A.A. (2020) Effect of Maximum Aggregate Size on the Strength of Normal and High Strength Concrete. *Civil Engineering Journal*, **6**, 1155-1165. https://doi.org/10.28991/cej-2020-03091537

[8] Malhotra, M. (1987) Supplementary Cementing Materials. CANMET Special Pub-

lication SP 86-8E, Energy, Mines and Resources. Ottawa.

[9] McCarthy, M.J. and Dyer, T.D. (2019) 9—Pozzolanas and Pozzolanic Materials. In: Hewlett, P.C. and Liska, M., Eds., *Lea's Chemistry of Cement and Concrete* (*Fifth Edition*), Butterworth-Heinemann, Oxford, 363-467. https://doi.org/10.1016/B978-0-08-100773-0.00009-5

[10] Metha, P.K. (1983) Mechanism of Sulfate Attack on Portland Cement Concrete—Another Look. *Cement and Concrete Research*, **13**, 401-406. https://doi.org/10.1016/0008-8846(83)90040-6

[11] Elahi, M.M.A., Shearer, C.R., Reza, A.N.R., Saha, A.K., Khan, M.N.N., Hossain, M.M. and Sarker, P.K. (2021) Improving the Sulfate Attack Resistance of Concrete by Using Supplementary Cementitious Materials (SCMs): A Review. *Construction and Building Materials*, **281**, Article ID: 122628. https://doi.org/10.1016/j.conbuildmat.2021.122628

[12] Rodriguez-Camacho, R.E. and Uribe-Afif, R. (2002) Importance of Using the Natural Pozzolans on Concrete Durability. *Cement and Concrete Research*, **32**, 1851-1858. https://doi.org/10.1016/S0008-8846(01)00714-1

[13] Binici, H., Yardim, Y., Aksogan, O., Resatoglu, R., Dincer, A. and Karrpuz, A. (2020) Durability Properties of Concretes Made with Sand and Cement Size Basalt. *Sustainable Materials and Technologies*, **23**, e00145. https://doi.org/10.1016/j.susmat.2019.e00145

[14] Mavonga, T., Zana, N. and Durrheim, R.J. (2010) Studies of Crustal Structure, Seismic Precursors to Volcanic Eruptions and Earthquake Hazard in the Eastern Provinces of the Democratic Republic of Congo. *Journal of African Earth Sciences*, **58**, 623-633. https://doi.org/10.1016/j.jafrearsci.2010.08.008

[15] Mulibo, G.D. (2022) Seismotectonics and Active Faulting of Usangu Basin, East African Rift System, with Implications for the Rift Propagation. *Tectonophysics*, **838**, Article ID: 229498. https://doi.org/10.1016/j.tecto.2022.229498

[16] Hertogen, J., Vanlerberghe, L. and Namegabe, M.R. (1985) Geochemical Evolution of the Nyiragongo Volcano (Virunga, Western African Rift, Zaire). *Bulletin of the Geological Society of Finland*, **57**, 21-35. https://doi.org/10.17741/bgsf/57.1-2.002

[17] Pitcavage, E., Furman, T., Nelson, W.R., Kalegga, P.K. and Barifaijo, E. (2021) Petrogenesis of Primitive Lavas from the Toro Ankole and Virunga Volcanic Provinces: Metasomatic Mineralogy beneath East Africa's Western Rift. *Lithos*, *396-397*, Article ID: 106192. https://doi.org/10.1016/j.lithos.2021.106192

[18] Furman, T. (2007) Geochemistry of East African Rift Basalts: An Overview. *Journal of African Earth Sciences*, **48**, 147-160. https://doi.org/10.1016/j.jafrearsci.2006.06.009

[19] Rooney, T.O. (2020) The Cenozoic Magmatism of East Africa: Part V-Magma Sources and Processes in the East African Rift. *Lithos*, *360-361*, Article ID: 105296. https://doi.org/10.1016/j.lithos.2019.105296

[20] Philippe, G., Michel, D. and Johannes, H. (1975) Contribution à l'étude géologique duvolcan Mikeno, Chaîne des Virunga (République du Zaïre). *Compte rendu des séances de la Société de physique et d'histoire naturelle de Genève*, **10**, 57-66.

[21] Pitcavage, E. (2020) Geochemical Investigations of Continental Rift Magmatism: A Case Study in East Africa's Western Rift. Master's Thesis, The Pennsylvania State University, State College.

[22] Furman, T. (2003) Geochemical Overview of the East African rift system. *AGU Fall Meeting Abstracts*, **2003**, S52G-03.

[23] Michon, L., Famin, V. and Quidelleur, X. (2022) Evolution of the East African Rift

System from Trap-Scale to Plate-Scale Rifting. *Earth-Science Reviews*, **231**, Article ID: 104089. https://doi.org/10.1016/j.earscirev.2022.104089

[24] Unčík, S. and Kmecová, V. (2013) The Effect of Basalt Powder on the Properties of Cement Composites. *Procedia Engineering*, **65**, 51-56. https://doi.org/10.1016/j.proeng.2013.09.010

[25] Shen, M., Zhou, L., Chen, Z., Shen, Y., Huang, B. and Lv, J. (2022) Effects of Basalt Powder and Silica Fume on Ultra-High-Strength Cementitious Matrix: A Comparative Study. *Case Studies in Construction Materials*, **17**, e01397. https://doi.org/10.1016/j.cscm.2022.e01397

[26] Dobiszewska, M., Pichór, W. and Szołdra, P. (2019) Effect of Basalt Powder Addition on Properties of Mortar. *MATEC Web of Conferences*, **262**, Article No. 06002. https://doi.org/10.1051/matecconf/201926206002

[27] Uysal, M. and Yilmaz, K. (2011) Effect of Mineral Admixtures on Properties of Self-Compacting Concrete. *Cement and Concrete Composites*, **33**, 771-776. https://doi.org/10.1016/j.cemconcomp.2011.04.005

[28] Abdelaziz, M.A., El-Aleem, S.A. and Menshawy, W.M. (2014) Effect of Fine Materials in Local Quarry Dusts of Limestone and Basalt on the Properties of Portland Cement Pastes and Mortars. *International Journal of Engineering Research*, **3**, 1038-1056.

[29] Amin, M., Sudibyo, S., Ordiana, A. and Karo, P. (2020) Effect of Basalt Mineral Concentration as PCC Cement Substitution Material on Mortar Products. *IOP Conference Series: Earth and Environmental Science*, **483**, Article ID: 012009. https://doi.org/10.1088/1755-1315/483/1/012009

[30] Berodier, E. (2015) Impact of the Supplementary Cementitious Materials on the Kinetics and Microstructural Development of Cement Hydration (No. 6417 THESIS). EPFL, Lausanne.

[31] Briki, Y. (2020) Maximizing the Use of Supplementary Cementitious Materials (SCMs) in Blended Cements (No. 8140 THESIS). EPFL, Lausanne.

[32] ASTM International (2023) Standard Specification for Coal Fly Ash and Raw or Calcined Natural Pozzolan for Use in Concrete.

[33] AFNOR (2018) Geotechnical Investigation and Testing—Laboratory Testing of Soil—Part 7: Unconfined Compression Test.

[34] AFNOR (2003) Mixing Water for Concrete—Specification for Sampling, Testing and Assessing the Suitability of Water, Including Water Recovered from Processes in the Concrete Industry, as Mixing Water for Concrete.

[35] American Society for Testing and Materials (2006) Standard Specification for Mixing Water Used in the Production of Hydraulic Cement Concrete. ASTM C1602/C1602M-06. https://www.astm.org/DATABASE.CART/HISTORICAL/C1602C1602M-06.htm

[36] AFNOR (2018) Methods of Testing Cement—Part 1: Determination of Strength. NF EN 196-1.

[37] AFNOR (2017) Methods of Testing Cement—Part 3: Determination of Setting Times and Soundness. NF EN 196-3.

[38] AFNOR (2017) NF EN 196-3. https://www.boutique.afnor.org/norme/nf-en-196-3/methodes-d-essai-des-ciments-par-tie-3-determination-du-temps-de-prise-et-de-la-stabilite/article/904098/fa186374

[39] AFNOR (2010) Testing Fresh Concrete—Part 6: Density. NF EN 192-6. Résistance à

la compression uniaxiale—NF EN 1926. Lithoscope. https://lithoscopectmnc.com/

[40] AFNOR (2010) Tests for Mechanical and Physical Properties of Aggregates—Part 2: Methods for the Determination of Resistance to Fragmentation. NF EN 1097-2.

[41] AFNOR (2020) Tests for Mechanical and Physical Properties of Aggregates—Part 2: Methods for the Determination of Resistance to Fragmentation. EN 1097-2, European Committee for Standardization, Brussels.

[42] Polat, Ö., Polat, A. and Ekici, T. (2021) Automatic Classification of Volcanic Rocks from Thin Section Images Using Transfer Learning Networks. *Neural Computing and Applications*, **33**, 11531-11540. https://doi.org/10.1007/s00521-021-05849-3

[43] Hattori, H. (1971) Preparation of Glass Disc Sample of Rock for Light Element Analysis by X-Ray Spectrometry. *Bulletin of the Geological Survey of Japan*, **22**, 103-116.

[44] Rohiman, A., Prijanto, D., *et al.* (2019) Geochemical Characteristics of Volcanic Rocks from Mt. Masurai's Caldera, Jambi, Indonesia. *Journal of Physics: Conference Series*, **1204**, 012070. https://doi.org/10.1088/1742-6596/1204/1/012070

[45] Rohiman, A. and Arifin, A.S. (2020) Comparation of Pressed Powder Pellet and Fused Glass Bead Preparation Techniques for Mayor Elements Analysis of Rock Samples Using X-Ray Fluorescence (XRF). *Indonesian Journal of Physics*, **31**, 24-27. https://doi.org/10.5614/itb.ijp.2020.31.2.4

[46] Spanu, D., Palestra, A., Prina, V., Monticelli, D., Bonanomi, S., Nanot, S.U., Binda, G., Rampazzi, L., Sessa, G., Callejo Munoz, D., *et al.* (2023) Tackling the Challenging Determination of Trace Elements in Ultrapure Silicon Carbide by LA-ICP-MS. *Molecules*, **28**, Article 2845. https://doi.org/10.3390/molecules28062845

[47] Ryoji, T. and Yuji, O. (1997) XRF Analysis of Major and Trace Elements for Silicate Rocks Using Low Dilution Ratio Fused Glass. *HUEPS Technical Report*, **2**, 1-20. http://hdl.handle.net/2115/62041

[48] Nuchdang, S., Channuie, J., Leelanupat, O. and Rattanaphra, D. (2019) Application of Handheld X-Ray Fluorescence Spectrometer for Major Element Analysis and Characterization of Geological Samples in Southern Thailand. *IOP Conference Series: Earth and Environmental Science*, **398**, Article ID: 012005. https://doi.org/10.1088/1755-1315/398/1/012005

[49] Willis, J., Feather, C. and Turner, K. (2014) Guidelines for XRF Analysis. James Willis Consultants, Cape Town.

[50] Chowdhury, A.R., Maheshwari, N., Soni, J., Kapil, M., Mehta, T. and Mukharya, A. (2020) Quantitative X-Ray Fluorescence Analysis: Trace Level Detection of Toxic Elemental Impurities in Drug Product by ED-XRF Spectrometer. *Journal of Pharmaceutical and Biomedical Analysis*, **189**, Article ID: 113292. https://doi.org/10.1016/j.jpba.2020.113292

[51] Vangu, S., Phuati, P., Eale, E., Lobota, M. and Ngimbi, M. (2022) Caracterisations Chimique et mineralogique aux Rayons x et Suivi de le Broyabilite des Clinker, Dolerite, Basalte et Metabasalte du Kongo-Central pour une Application Cimentiere. *ACASTI and CEDESURK Online JOURNAL*, **10**, 11-23.

[52] Taylor, H.F.W. (1997) Cement Chemistry. Thomas Telford, London. https://doi.org/10.1680/cc.25929

[53] Dorn, T., Blask, O. and Stephan, D. (2022) Acceleration of Cement Hydration—A Review of the Working Mechanisms, Effects on Setting Time, and Compressive Strength Development of Accelerating Admixtures. *Construction and Building Materials*, **323**, Article ID: 126554. https://doi.org/10.1016/j.conbuildmat.2022.126554

[54] Harrisson, A.M. (2019) 4—Constitution and Specification of Portland Cement. In: Hewlett, P.C. and Liska, M., *Lea's Chemistry of Cement and Concrete* (*Fifth Edition*), Butterworth-Heinemann, Oxford, 87-155. https://doi.org/10.1016/B978-0-08-100773-0.00004-6

[55] Locher, F.W. (2013) Cement: Bau + Technik GmbH. https://www.perlego.com/book/1035680/cement-principles-of-production-and-use-pdf

[56] Sadrmomtazi, A., Tajasosi, S. and Tahmouresi, B. (2018) Effect of Materials Proportion on Rheology and Mechanical Strength and Microstructure of Ultra-High Performance Concrete (UHPC). *Construction and Building Materials*, **187**, 1103-1112. https://doi.org/10.1016/j.conbuildmat.2018.08.070

[57] Rikoto, I.I. and Nuhu, S. (2019) Effect of Free Lime and Lime Saturation Factor on Grindability of Cement Clinker. *International Journal of Engineering Research and Reviews,* **7**, 61-66.

[58] Horckmans, L., Möckel, R., Nielsen, P., Kukurugya, F., Vanhoof, C., Morillon, A. and Algermissen, D. (2019) Multi-Analytical Characterization of Slags to Determine the Chromium Concentration for a Possible Re-Extraction. *Minerals*, **9**, Article 646. https://doi.org/10.3390/min9100646

[59] Le, V.S., Louda, P., Tran, H.N., Nguyen, P.D., Bakalova, T., Ewa Buczkowska, K. and Dufkova, I. (2020) Study on Temperature-Dependent Properties and Fire Resistance of Metakaolin-Based Geopolymer Foams. *Polymers*, **12**, Article 2994. https://doi.org/10.3390/polym12122994

[60] Zhao, Y., Zhang, Z., Ji, Y., Song, L. and Ma, M. (2023) Experimental Research on Improving Activity of Calcinated Coal Gangue via Increasing Calcium Content. *Materials*, **16**, Article 2705. https://doi.org/10.3390/ma16072705

[61] Baby-Jean Robert Mungyeko, B. and Marias, F. (2019) Modeling of Cement Clinker Chemistry and Engineering of Cement Manufacturing Process: State of the Art. *International Journal of Innovation and Applied Studies,* **25**, 528-551.

[62] Hewlett, P.C. and Liska, M. (2019) Lea's Chemistry of Cement and Concrete. Butterworth-Heinemann, Oxford.

[63] Bresciani, C. (2008) Simulation numérique de l'hydratation et du développement des propriétés physiques et mécaniques d'une pâte de ciment afin de sélectionner de nouveaux ajouts minéraux. Master's Thesis, École des Mines de Paris—Université PSL, Paris.

[64] Dolenec, S., Šter, K., Borštnar, M., Nagode, K., Ipavec, A. and Žibret, L. (2020) Effect of the Cooling Regime on the Mineralogy and Reactivity of Belite-Sulfoaluminate Clinkers. *Minerals*, **10**, Article 910. https://doi.org/10.3390/min10100910

[65] Shim, S.H., Lee, T.H., Yang, S.J., Noor, N.B.M. and Kim, J.H.J. (2021) Calculation of Cement Composition Using a New Model Compared to the Bogue Model. *Materials*, **14**, Article 4663. https://doi.org/10.3390/ma14164663

[66] Le Bas, M.J., Le Maitre, R.W., Streckeisen, A., Zanettin, B. and IUGS Subcommission on the Systematics of Igneous Rocks (1986) A Chemical Classification of Volcanic Rocks Based on the Total Alkali-Silica Diagram. *Journal of Petrology*, **27**, 745-750. https://doi.org/10.1093/petrology/27.3.745

[67] El-Desoky, H., Abd El-Hafez, N., Khalil, A., Arafat, A., Hasan, M.G. and Youssef, T. (2023) The Geology, Petrography, and Geochemistry of Egyptian Dokhan Volcanics: A Potential Source for Construction Aggregate. *Minerals*, **13**, Article 635. https://doi.org/10.3390/min13050635

[68] Le Bas, M.J. (2000) IUGS Reclassification of the High-Mg and Picritic Volcanic Rocks. *Journal of Petrology*, **41**, 1467-1470. https://doi.org/10.1093/petrology/41.10.1467

[69] Yan, D., Chu, Z., Liu, Z., Wang, W. and Xiong, F. (2023) Petrogenesis of Early Triassic Felsic Volcanic Rocks in the East Kunlun Orogen, Northern Tibet: Implications for the Paleo-Tethyan Tectonic and Crustal Evolution. *Minerals*, **13**, Article 607. https://doi.org/10.3390/min13050607

[70] Shi, K., Yang, X., Du, J., Cao, J., Wan, Q. and Cai, Y. (2020) Geochemical Study of Cretaceous Magmatic Rocks and Related Ores of the Hucunnan Cu-Mo Deposit: Implications for Petrogenesis and Poly-Metal Mineralization in the Tongling Ore-Cluster Region. *Minerals*, **10**, Article 107. https://doi.org/10.3390/min10020107

[71] Minissale, S., Casalini, M., Cucciniello, C., Balagizi, C., Tedesco, D., Boudoire, G., Morra, V. and Melluso, L. (2022) The Geochemistry of Recent Nyamulagira and Nyiragongo Potassic Lavas, Virunga Volcanic Province, and Implications on the Enrichment Processes in the Mantle Lithosphere of the Tanzania-Congo Craton. *Lithos*, **420-421**, Article ID: 106696. https://doi.org/10.1016/j.lithos.2022.106696

[72] Cross, W., Iddings, J.P., Pirsson, L.V. and Washington, H.S. (1902) A Quantitative Chemico-Mineralogical Classification and Nomenclature of Igneous Rocks. *The Journal of Geology*, **10**, 555-690. https://doi.org/10.1086/621030

[73] Shi, L., Ju, N., Feng, Y., Zheng, C., Wu, Y. and Liu, X. (2023) Petrogenesis and Tectonic Setting of the Early and Middle Jurassic Granitoids in the Chaihe Area, Central Great Xing'an Range, NE China. *Minerals*, **13**, Article 917. https://doi.org/10.3390/min13070917

[74] Chen, X., Zhang, Y., Huo, H. and Wu, Z. (2020) Study of High Tensile Strength of Natural Continuous Basalt Fibers. *Journal of Natural Fibers*, **17**, 214-222. https://doi.org/10.1080/15440478.2018.1477087

[75] González-Guzmán, R., Elizondo-Pacheco, L.A., González-Roque, A., *et al.* (2023) ShinyNORRRM: A Cross-Platform Software to Calculate the CIPW Norm. *Mathematical Geosciences*, **55**, 563-577. https://doi.org/10.1007/s11004-023-10052-2

[76] Pouclet, A. and Bram, K. (2021) Nyiragongo and Nyamuragira: A Review of Volcanic Activity in the Kivu Rift, Western Branch of the East African Rift System. *Bulletin of Volcanology*, **83**, Article No. 10. https://doi.org/10.1007/s00445-021-01435-6

[77] Zhu, Y., Li, Y., Ding, H., *et al.* (2022) Vibrational and Structural Insight into Silicate Minerals by Mid-Infrared Absorption and Emission Spectroscopies. *Physics and Chemistry of Minerals*, **49**, Article No. 6. https://doi.org/10.1007/s00269-022-01180-y

[78] Sapei, Lanny (2007) Characterisation of Silica in *Equisetum hyemale* and Its Transformation into Biomorphous Ceramics. Thèse de Doctorat, Universität Potsdam, Potsdam. https://publishup.uni-potsdam.de/opus4-ubp/frontdoor/index/index/docId/609

[79] Seroka, N.S., Taziwa, R. and Khotseng, L. (2022) Green Synthesis of Crystalline Silica from Sugarcane Bagasse Ash: Physico-Chemical Properties. *Nanomaterials*, **12**, Article 2184. https://doi.org/10.3390/nano12132184

[80] Xu, J., Wang, C., Wang, T., Wang, Y., Kang, Q., Liu, Y. and Tian, Y. (2018) Mechanisms for Low-Temperature Direct Bonding of Si/Si and Quartz/Quartz *via* VUV/O_3 Activation. *RSC Advances*, **8**, 11528-11536. https://doi.org/10.1039/C7RA13095C

[81] Trease, N.M., Clark, T.M., Grandinetti, P.J., Stebbins, J.F. and Sen, S. (2017) Bond

Length-Bond Angle Correlation in Densified Silica—Results from ^{17}O NMR Spectroscopy. *The Journal of Chemical Physics*, **146**, Article ID: 184505. https://doi.org/10.1063/1.4983041

[82] Stein, M. and Schaller, J. (2022) Comparing Amorphous Silica, Short-Range-Ordered Silicates and Silicic Acid Species by FTIR. *Scientific Reports*, **12**, Article No. 11708. https://doi.org/10.1038/s41598-022-15882-4

[83] Jozanikohan, G. and Abarghooei, M.N. (2022) The Fourier Transform Infrared Spectroscopy (FTIR) Analysis for the Clay Mineralogy Studies in a Clastic Reservoir. *Journal of Petroleum Exploration and Production Technology*, **12**, 2093-2106. https://doi.org/10.1007/s13202-021-01449-y

[84] Erhard, L.C., Rohrer, J., Albe, K. and Deringer, V.L. (2022) A Machine-Learned Interatomic Potential for Silica and Its Relation to Empirical Models. *npj Computational Materials*, **8**, Article No. 90. https://doi.org/10.1038/s41524-022-00768-w

[85] Sherpa, L.S. (2021) Failure Analysis of Injection Moulded Parts. https://www.theseus.fi/handle/10024/503950

[86] Adomako, S., Engelsen, C.J., Thorstensen, R.T. and Barbieri, D.M. (2021) Review of the Relationship between Aggregates Geology and Los Angeles and Micro-Deval Tests. *Bulletin of Engineering Geology and the Environment*, **80**, 1963-1980. https://doi.org/10.1007/s10064-020-02097-y